Numerical study for boundary layer flows of Maxwell fluid with heat and mass transfer effects

by

Zubaida Shafique

A dissertation submitted in partial fulfillment of the requirements

for the degree of Master of Philosophy in Mathematics

Supervised by

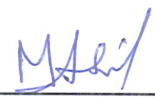## Dr. Meraj Mustafa Hashmi

School of Natural Sciences,

National University of Sciences and Technology,
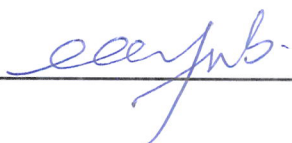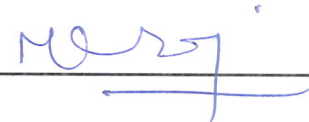
Islamabad, Pakistan

2016

National University of Sciences & Technology

MASTER'S THESIS WORK

We hereby recommend that the dissertation prepared under our supervision by: Zubaida Shafique, Regn No. NUST201463617MSNS78014F Titled: Numerical Study for Boundary Layer Flows of Maxwell Fluid with Heat and Mass Transfer Effects be accepted in partial fulfillment of the requirements for the award of **MS** degree.

Examination Committee Members

1. Name: Dr. Yousaf Habib   Signature: _Yousaf Habib_

2. Name: Dr. Muhammad Asif Farooq   Signature: _Asif_

3. Name: _____   Signature: _____

4. Name: Prof. Muhammad Ayub   Signature: _____

Supervisor's Name: Dr. Meraj Mustafa Hashmi   Signature: _____

_____
Head of Department

04-11-2016
Date

COUNTERSINGED

Date: 04/11/16

_____
Dean/Principal

Dedication

To my loving father and mother

Acknowledgment

First and foremost, I am highly grateful to Allah Almighty for blessing me health, knowledge and courage to complete my goals. I invoke peace for the Holy Prophet Muhammad (PBUH) who is the torch of guidance and inspiration for all the mankind in all times.

I pay my sincere gratitude to my supervisor Dr. Meraj Mustafa Hashmi, Assistant Professor, (SNS) NUST for his persistant guidance and valuable time. It is because of his versatile technique of teaching that I have completed my research in time. I express my thanks to my GEC members, Dr. Muhammad Asif Farooq (SNS) NUST and Dr. Yousaf Habib (SNS) NUST for their thoughtful suggestions and valuable advices. I also place on record my thanks to Dr. Ammar Mushtaq (RCMS), NUST who helped me out in programming in MATLAB.

Above ground, I am under the obligation of my parents, my sisters Ayesha and Khadija and my brother Anees for their love and unconditional support. They always encourage me to give my best. Extending my appreciation, I would also like to acknowledge all my friends and colleagues who created a positive and genial environment for this laborious research to be completed.

I am thankful to everyone who helped me directly or indirectly in this venture.

Zubaida Shafique

Abstract

The analysis of boundary layer flow past a stretching surface is of great importance in many technological and industrial processes such as paper production, glass fiber, extrusion of plastic sheets and hot rolling etc. Viscoelastic fluids comprise a variety of industrial and house hold products such as polymers, dough used to make bread and pasta, toothpaste and paints etc. Here we study the heat/mass transfer effects on the revolving flow of Maxwell fluid due to unidirectional stretching surface. Mass transfer process is modeled in terms of binary chemical reaction and activation energy. Modified Arrhenius function for activation energy is invoked. Traditional boundary layer approximations are utilized to simplify the governing equations. By similarity transformation, we obtain a self-similar form of boundary layer equations which are solved numerically. The solutions depend on interesting parameters such as the rotation parameter λ, the Deborah number β, the Prandtl number $\Pr$, the Schmidt number Sc, activation energy E, fitted rate constant n and temperature difference parameter δ. We found that the solute concentration in binary mixture is proportional to both rotation parameter λ and activation energy E. The reaction rate σ and fitted rate n both tend to reduce the solute concentration. Thermal boundary layer becomes thicker and heat transfer rate diminishes when fluid is subjected to larger rotation rate.

CONTENTS

Chapter 1

Introduction

1.1 Basic definitions

Fluids can be classified as either Newtonian or non-Newtonian depending on their rheological behavior.

1.1.1 Newtonian fluids

In these fluids shear stress τ_{yx} is directly and linearly proportional to the shear rate $\dot{\gamma}_{yx}$. For a laminar flow over a flat moving plate, shear rate can be expressed as velocity gradient $\dfrac{dV_x}{dy}$ in the direction perpendicular to the shearing force. Mathematically,

$$\tau_{yx} = \mu \frac{dV_x}{dy} = \mu \dot{\gamma}_{yx}, \tag{1.1}$$

where μ is the coefficient of viscosity also called dynamic viscosity. The graph of τ_{yx} verses $\dot{\gamma}_{yx}$ is a straight line whose slope μ is passing through the origin.

1.1.2 Non-Newtonian fluid

In contrast to the Newtonian fluids, the ratio of shear stress and shear rate is not constant in non-Newtonian fluids for the given pressure and temperature and depends on flow condition such as deformation history, shear rate and geometry of the fluid element under consideration. The flow curve for non-Newtonian fluid is non-linear and it generally does not pass through the origin.

The flow of non-Newtonian fluids can be explained mathematically by the power law model which is given as

$$\tau_{yx} = K(\dot{\gamma})^n, \tag{1.2}$$

$$\eta = \frac{\tau_{yx}}{\dot{\gamma}} = K(\dot{\gamma})^{n-1}, \tag{1.3}$$

here K is the consistency index, n the flow behavior index and η the apparent viscosity.

For $n < 1$ the fluid demonstrates shear-thinning properties, for $n = 1$ the fluid shows Newtonian behavior and for $n > 1$ the fluid represents shear-thickening behavior.

1.1.3 Incompressible and compressible flows

The fluid whose specific volume V is a function of pressure, is called a compressible fluid. All gases are considered as compressible fluids.

On contrary, an incompressible fluid is a fluid whose density remains unchanged by the external forces applied on it. Liquids are considered as incompressible fluids under the condition of normal pressure.

Classification of compressible and incompressible flows can be made on the basis of Mach number. If the Mach number (the ratio of flow velocity to the velocity of sound) is less than 0.3, the flow is considered as incompressible and if this ratio is greater than 0.3 the flow is considered as compressible.

1.1.4 Coriolis acceleration

The additional acceleration experienced by the body moving in a rotating frame of reference with constant velocity is called coriolis acceleration. It is the second pseudo force that opposes the retarding force and causes the path to be appeared as curve with respect to the rotating frame of reference. Mathematically, it is expressed below:

2

$$\mathbf{a}_{cor} = -2\mathbf{\Omega} \times \mathbf{V}, \tag{1.4}$$

here $\mathbf{\Omega}$ is the angular velocity and $\mathbf{V}$ is the velocity field. Its direction is right to the velocity vector if $\mathbf{\Omega}$ is anti-clock wise.

1.1.5 Centrifugal acceleration

It is a reaction force that ensures the motion of body in circular path without falling in to the center. It is directed radially outward and is given as

$$\mathbf{\Omega} \times (\mathbf{\Omega} \times \mathbf{r}) = -\nabla \left(\frac{\Omega^2 r^2}{2} \right), \tag{1.5}$$

where $\mathbf{r}$ is the radius vector of the circular path.

1.1.6 Deborah number

Deborah number is defined as the ratio of the stress relaxation time t_c to the characteristic time scale t_p. It is denoted by De and given as

$$De = \frac{t_c}{t_p}. \tag{1.6}$$

A material with small Deborah number behaves as fluid like material while the material with large Deborah number shows the properties of solid like material.

1.1.7 Reynolds number

The ratio of the inertial forces to the viscous forces is defined as Reynolds number. Mathematically,

$$Re = \frac{\rho VL}{\mu}, \tag{1.7}$$

3

where L is the characteristic length, ρ the density, V the mean velocity and μ the dynamic viscosity of the fluid. Reynolds number determines the nature of the flow. If $\mathrm{Re} \leq 2300$ the flow will be laminar, if $2300 < \mathrm{Re} \leq 4000$ the flow is in transition state and if $\mathrm{Re} > 4000$ the flow is turbulent.

1.1.8 Prandtl number

The ratio of kinematic viscosity ν to the thermal diffusivity α is named as Prandtl number. It is denoted by Pr. Thus

$$\mathrm{Pr} = \frac{\nu}{\alpha}. \tag{1.8}$$

When the value of Pr is small, it means that heat diffuses quickly as compared to the momentum while for large value of Pr, momentum diffusivity dominates the thermal behavior.

1.1.9 Schmidt number

The ratio of momentum diffusivity ν to mass diffusivity D is called as Schmidt number. It is given as

$$Sc = \frac{\nu}{D}. \tag{1.9}$$

It is analogous to Prandtl number in heat transfer and compares the relative thicknesses of hydrodynamics and concentration boundary layers.

1.1.10 Nusselt number

Nusselt number also referred as heat transfer coefficient is the ratio of heat transfer due to convection to heat transfer due to conduction. Mathematically,

4

$$Nu = \frac{xq_w}{k\Delta T},$$ (1.10)

where $q_w = -k \left. \frac{\partial T}{\partial z} \right|_{z=0}$ is the wall heat flux and $\Delta T = T_w - T_\infty$ is the temperature difference between the surface and the free stream.

1.1.11 Sherwood number

Sherwood number also referred as mass transfer coefficient is the ratio of mass transfer due to convection to mass transfer due to diffusion. Mathematically,

$$Sh = \frac{xj_w}{D\Delta C},$$ (1.11)

where $j_w = -D \left. \frac{\partial C}{\partial z} \right|_{z=0}$ is the wall mass flux and $\Delta C = C_w - C_\infty$ is the concentration difference between species in the mixture.

1.1.12 Boundary layer

The fine region in the neighborhood of an object merged in the fluid is called a boundary layer. By the boundary layer theory, the flow past a body is contained in two forms, a main stream referred as ideal stream where the effects of viscosity and thermal conductivity are negligible and a thin layer near the surface where the fluid is regarded as viscous and thermally conductive. These inviscid and viscous flows balance each other at the outer edge of the boundary layer. Due to the sufficient viscosity and thermal conductivity the velocity and thermal gradients are also large which give a thin boundary layer with respect to the scale of the flow.
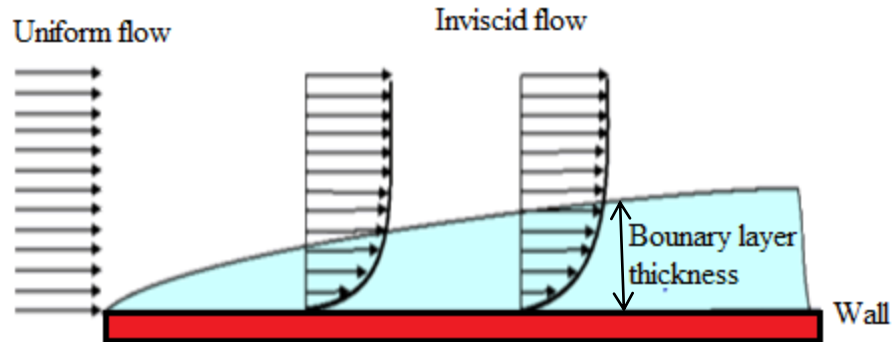
Fig. 1.1. Boundary layer for velocity

Variation in pressure and velocity can bring changes in the flow pattern of a fluid. On the basis of the flow pattern, a flow may be laminar or turbulent.

1.1.13 Turbulent flow

Turbulent flow is classified by eddies and whirls caused by irregular motion and superimposed velocity fluctuations on the average flow due to chaotic pressure and velocity changes. This type of flows is linked with high Reynolds number due to the dominance of inertial forces on viscous forces.

1.1.14 Laminar flow

In contrast to the turbulent flow, laminar flow is well ordered and regular in its motion. It consists of streamlines that slide parallel with each other with respect to its neighbor. Laminar flows are associated with low Reynolds number where the viscous forces dominate and cause the velocity to decrease and fluid flows without mixing between the layers.

1.2 Boundary layer equation for a rotating flow of Maxwell fluid

The constitutive equations for flow of Maxwell fluid in rotating frame are

$$\nabla.\mathbf{V} = 0, \tag{1.12}$$

$$\rho\left[(\mathbf{V}.\nabla)\mathbf{V} + \mathbf{\Omega} \times (\mathbf{\Omega} \times \mathbf{r}) + 2\mathbf{\Omega} \times \mathbf{V}\right] = -\nabla p + \nabla.\,\mathbf{S}, \tag{1.13}$$

$$\mathbf{S} + \lambda_1 \frac{D\mathbf{S}}{Dt} = \mu \mathbf{A}_1, \tag{1.14}$$

where ρ is the density of the fluid, $\mathbf{V} = \left[u(x,y,z), v(x,y,z), w(x,y,z)\right]$ is the velocity vector, $\mathbf{\Omega}$ is angular velocity of the fluid, $\mathbf{r}$ is the radius vector, $\mathbf{S}$ is extra stress tensor, λ_1 is the fluid relaxation time, D/Dt is the convected time derivative, μ is the dynamic viscosity and $\mathbf{A}_1$ is the first Rivlin-Erickson tensor which is represented as

$$\mathbf{A}_1 = \nabla\mathbf{V} + (\nabla\mathbf{V})^t, \tag{1.15}$$

$$= \begin{bmatrix} 2\dfrac{\partial u}{\partial x} & \dfrac{\partial u}{\partial y} + \dfrac{\partial v}{\partial x} & \dfrac{\partial u}{\partial z} + \dfrac{\partial w}{\partial x} \\[2ex] \dfrac{\partial u}{\partial y} + \dfrac{\partial v}{\partial x} & 2\dfrac{\partial v}{\partial y} & \dfrac{\partial v}{\partial z} + \dfrac{\partial w}{\partial y} \\[2ex] \dfrac{\partial u}{\partial x} + \dfrac{\partial w}{\partial z} & \dfrac{\partial v}{\partial x} + \dfrac{\partial w}{\partial z} & 2\dfrac{\partial w}{\partial z} \end{bmatrix}. \tag{1.16}$$

For any vector a_i, the convected derivative D/Dt is given by

$$\frac{Da_i}{Dt} = \frac{\partial a_i}{\partial t} + \mathbf{V}_r a_{i,r} - \mathbf{V}_{i,r} a_r. \tag{1.17}$$

Taking $\mathbf{\Omega} = (0,0,\Omega)$ and $\mathbf{r} = (x,y,0)$, we expressed centrifugal acceleration as

$$\mathbf{\Omega} \times (\mathbf{\Omega} \times \mathbf{r}) = -\nabla\left(\frac{\Omega^2 r^2}{2}\right). \tag{1.18}$$

Using Eq. (1.18) in Eq. (1.13) we have,

$$\rho\left[(\mathbf{V}.\nabla)\mathbf{V} + 2\mathbf{\Omega} \times \mathbf{V}\right] = -\nabla\left(p - \rho\frac{\Omega^2 r^2}{2}\right) + \nabla.\,\mathbf{S}. \tag{1.19}$$

7

Now defining modified pressure as $\hat{p} = p - \rho \dfrac{\Omega^2 r^2}{2}$ and using Eq. (1.18), Eq. (1.13) takes the following form

$$\rho\left[(\mathbf{V}.\nabla)\mathbf{V} + 2\mathbf{\Omega}\times\mathbf{V}\right] = -\nabla\hat{p} + \nabla.\,\mathbf{S}. \tag{1.20}$$

Assigning the operator $\left(1 + \lambda_1\dfrac{D}{Dt}\right)$ on both side of Eq. (1.20), we obtain

$$\rho\left(\left(1 + \lambda_1\frac{D}{Dt}\right)(\mathbf{V}.\nabla)\mathbf{V} + \left(1 + \lambda_1\frac{D}{Dt}\right)(2\mathbf{\Omega}\times\mathbf{V})\right) = -\left(1 + \lambda_1\frac{D}{Dt}\right)\nabla\hat{p} + \left(1 + \lambda_1\frac{D}{Dt}\right)(\nabla.\,\mathbf{S}), \tag{1.21}$$

where

$$\frac{D}{Dt}(\nabla.) = \nabla.\left(\frac{D}{Dt}\right). \tag{1.22}$$

Implementing Eq. (1.22) on Eq. (1.21) and then using Eq. (1.14), we get

$$\rho\left(\left(1 + \lambda_1\frac{D}{Dt}\right)(\mathbf{V}.\nabla)\mathbf{V} + \left(1 + \lambda_1\frac{D}{Dt}\right)(2\mathbf{\Omega}\times\mathbf{V})\right) = -\left(1 + \lambda_1\frac{D}{Dt}\right)\nabla\hat{p} + \nabla.\left(1 + \lambda_1\frac{D}{Dt}\right)\mathbf{S}, \tag{1.23}$$

$$= -\left(1 + \lambda_1\frac{D}{Dt}\right)\nabla\hat{p} + \mu(\nabla.\mathbf{A}_1). \tag{1.24}$$

In the absence of the pressure gradient, Eq. (1.24) becomes

$$\rho\left(\left(1 + \lambda_1\frac{D}{Dt}\right)(\mathbf{V}.\nabla)\mathbf{V} + \left(1 + \lambda_1\frac{D}{Dt}\right)(2\mathbf{\Omega}\times\mathbf{V})\right) = \mu(\nabla.\mathbf{A}_1). \tag{1.25}$$

The components of Eq. (1.25) are as follows

8

$$u\frac{\partial u}{\partial x}+v\frac{\partial u}{\partial y}+w\frac{\partial u}{\partial z}-2v\Omega=v\left(\frac{\partial^2 u}{\partial x^2}+\frac{\partial^2 u}{\partial y^2}+\frac{\partial^2 u}{\partial z^2}\right)-\lambda_1\begin{pmatrix}u^2\dfrac{\partial^2 u}{\partial x^2}+v^2\dfrac{\partial^2 u}{\partial y^2}+w^2\dfrac{\partial^2 u}{\partial z^2}+2uv\dfrac{\partial^2 u}{\partial x\partial y}\\[2mm]+2vw\dfrac{\partial^2 u}{\partial y\partial z}+2wu\dfrac{\partial^2 u}{\partial z\partial x}-2u\Omega\dfrac{\partial v}{\partial x}-2v\Omega\dfrac{\partial v}{\partial y}\\[2mm]-2w\Omega\dfrac{\partial v}{\partial z}+2v\Omega\dfrac{\partial u}{\partial x}-2u\Omega\dfrac{\partial u}{\partial y}\end{pmatrix}\quad(1.26)$$

$$u\frac{\partial v}{\partial x}+v\frac{\partial v}{\partial y}+w\frac{\partial v}{\partial z}+2u\Omega=v\left(\frac{\partial^2 v}{\partial x^2}+\frac{\partial^2 v}{\partial y^2}+\frac{\partial^2 v}{\partial z^2}\right)-\lambda_1\begin{pmatrix}u^2\dfrac{\partial^2 v}{\partial x^2}+v^2\dfrac{\partial^2 v}{\partial y^2}+w^2\dfrac{\partial^2 v}{\partial z^2}+2uv\dfrac{\partial^2 v}{\partial x\partial y}\\[2mm]+2vw\dfrac{\partial^2 v}{\partial y\partial z}+2wu\dfrac{\partial^2 v}{\partial z\partial x}+2u\Omega\dfrac{\partial u}{\partial x}+2v\Omega\dfrac{\partial u}{\partial y}\\[2mm]+2w\Omega\dfrac{\partial u}{\partial z}+2v\Omega\dfrac{\partial v}{\partial x}-2u\Omega\dfrac{\partial v}{\partial y}\end{pmatrix}.\quad(1.27)$$

Using the boundary layer approximations, Eq. (1.26) and Eq. (1.27) become

$$u\frac{\partial u}{\partial x}+v\frac{\partial u}{\partial y}+w\frac{\partial u}{\partial z}-2v\Omega=v\frac{\partial^2 u}{\partial z^2}-\lambda_1\begin{pmatrix}u^2\dfrac{\partial^2 u}{\partial x^2}+v^2\dfrac{\partial^2 u}{\partial y^2}+w^2\dfrac{\partial^2 u}{\partial z^2}+2uv\dfrac{\partial^2 u}{\partial x\partial y}\\[2mm]+2vw\dfrac{\partial^2 u}{\partial y\partial z}+2wu\dfrac{\partial^2 u}{\partial z\partial x}-2u\Omega\dfrac{\partial v}{\partial x}-2v\Omega\dfrac{\partial v}{\partial y}\\[2mm]-2w\Omega\dfrac{\partial v}{\partial z}+2v\Omega\dfrac{\partial u}{\partial x}-2u\Omega\dfrac{\partial u}{\partial y}\end{pmatrix},\quad(1.28)$$

$$u\frac{\partial v}{\partial x}+v\frac{\partial v}{\partial y}+w\frac{\partial v}{\partial z}+2u\Omega=v\frac{\partial^2 v}{\partial z^2}-\lambda_1\begin{pmatrix}u^2\dfrac{\partial^2 v}{\partial x^2}+v^2\dfrac{\partial^2 v}{\partial y^2}+w^2\dfrac{\partial^2 v}{\partial z^2}+2uv\dfrac{\partial^2 v}{\partial x\partial y}\\[2mm]+2vw\dfrac{\partial^2 v}{\partial y\partial z}+2wu\dfrac{\partial^2 v}{\partial z\partial x}+2u\Omega\dfrac{\partial u}{\partial x}+2v\Omega\dfrac{\partial u}{\partial y}\\[2mm]+2w\Omega\dfrac{\partial u}{\partial z}+2v\Omega\dfrac{\partial v}{\partial x}-2u\Omega\dfrac{\partial v}{\partial y}\end{pmatrix}.\quad(1.29)$$

1.3 Conservation of energy

The constitutive energy equation in the absence of viscous dissipation and heat generation/absorption and under the constant pressure is given as

$$\rho\, c_p\, (\mathbf{V}.\nabla)T = -\nabla.\, \mathbf{q}, \tag{1.30}$$

where ρ is the fluid density, c_p is specific heat, $\mathbf{V} = \left[u(x,y,z), v(x,y,z), w(x,y,z)\right]$ is the velocity vector, T is the temperature of the fluid and $\mathbf{q}$ is the heat flux which by the Fourier's law of heat conduction is given as

$$\mathbf{q} = -k\nabla T, \tag{1.31}$$

where k is the thermal conductivity. By using Eq. (1.31) in Eq. (1.30) we get

$$(\mathbf{V}.\nabla)T = \alpha\nabla^2 T, \tag{1.32}$$

where $\alpha = k/\rho c_p$ is the thermal diffusivity. Utilizing the boundary layer approximations, Eq. (1.32) in component form reduces to

$$u\frac{\partial T}{\partial x} + v\frac{\partial T}{\partial y} + w\frac{\partial T}{\partial z} = \alpha\left(\frac{\partial^2 T}{\partial x^2} + \frac{\partial^2 T}{\partial y^2} + \frac{\partial^2 T}{\partial z^2}\right). \tag{1.33}$$

1.4 Conservation of mass

Activation energy is defined as the least obligatory amount of energy for atoms or molecules to bring themselves in a state in which they can undergo a chemical reaction. Some chemical reactions proceed faster at high temperature. Svante Arrhenius represented the Arrhenius equation which is the quantitative relationship between rate of reaction and its temperature. It is given as

$$k = A\exp\left(-\frac{E_a}{\kappa(T - T_\infty)}\right), \tag{1.34}$$

where k is the rate constant of chemical reaction, A is the pre exponential factor, E_a is the activation energy, $\kappa = 8.61 \times 10^{-5}\, eV/K$ is the Boltzmann constant and T is the temperature

(in kelvin). High temperature increases the collisions between the molecules which increase the kinetic energy and thus the activation energy is affected.

The constitutive equation of mass transfer for Maxwell fluid in the presence of a binary chemical reaction and activation energy is given as

$$(\mathbf{V}.\nabla C) = D\nabla^2 C - k_r^2 \left(\frac{T}{T_\infty}\right)^n e^{-\frac{E_a}{\kappa T}}(C - C_\infty), \tag{1.35}$$

where C represents the concentration field and D the solute diffusivity. The term $k_r^2 \left(T/T_\infty\right)^n \exp(-E_a/\kappa T)$ is the modified Arrhenius function [11], κ is the Boltzmann constant, k_r^2 the reaction rate and n the fitted rate constant generally lies in $-1 < n < 1$.

1.5 Literature survey

Mass transfer is a natural phenomenon in many processes such as absorption, vaporization and condensation in a mixture, diffusion of nutrients in tissues, thermal insulation, cooling towers and food processing, in absorbers such as activated carbon beds and in the condensation process, dispersion of temperature/moisture over groove fields and distillation of alcohol. Mass transfer has relevance in most living-matter processes such as respiration, nutrition, sweating etc. Mass transfer process with chemical reaction has been given special attention in the past (see [1] - [6] and ref. there in) because of its significance in chemical engineering, geothermal reservoirs, nuclear reactor cooling and thermal oil recovery. Bestman [7] was probably the first to study the boundary layer flow involving the binary chemical reaction. He analytically examined the effects of the activation energy on natural convection flow in a porous medium by using perturbation approach. One of the factors that have an important role in chemical reaction is the activation energy. It is defined as the least obligatory amount of energy for atoms or molecules to bring themselves in a state in which they can undergo a chemical reaction. The concept of activation energy is usually applicable in areas pertaining to geothermal or oil reservoir engineering and

mechanics of water and oil emulsions. Activation energy can be realized as energy barrier that separates two minima of potential energy (of the reactants and products of a reaction) which has to be overcome by reactants to initiate a chemical reaction. Makinde et al. [8] presented the numerical solution for unsteady convection flow over a flat porous plate with n^{th} order chemical reaction and Arrhenius activation energy. The recent attempts in this direction were made by Maleque [9], [10] who investigated the influence of binary chemical reaction with Arrhenius activation energy on mixed convection flows and Awad et al. [11] who explored the unsteady revolving flow due to impulsively stretched plate by means of spectral relaxation method (SRM).

Steady and unsteady rotating flows have several noteworthy applications in geophysical and chemical fluid dynamics. They are also of applied significance in many areas such as in food processing, in rotor-stator systems, in thermal-power generating systems, in rotating machinery and in the cooling of the skins of high speed aircrafts. Wang [12] firstly explored the mathematical model for the effects of rotation on fluid flow adjacent to a stretched plate. In his work analytical solutions of velocity and temperature profiles were derived by perturbation approach. Effects of magnetic field on rotating fluid flow on stretching plate were observed by Takhar et al. [13]. Nazar et al. [14] employed similarity approach to examine unsteady revolving flow by an impulsively stretching plate. Kumari et al. [15] considered the flow near a stretching plate in revolving power-law and derived numerical approximations for both pseudoplastic and dilatant type fluids. Local similarity solutions for rotating viscous flow due to exponentially stretching plate were obtained by Javed et al. [16] utlizing Keller-box method. Zaimi et al. [17] considered a stretching surface immersed in rotating Walters' B liquid. Mustafa [18] analytically studied the rotating flow of viscoelastic fluid bounded by a stretching surface through Cattaneo-Christov heat flux theory. Turkyilmazoglu [19] extended the traditional Bödewadt flow problem for uniformly stretching disk. His numerical solution through collection method showed that radial stretching of disk improves the cooling process in practical applications. Mustafa et al. [20] also studied the Bödewadt flow problem over a stretching disk utilizing nanofluids. Numerical simulations for rotating flow of water containing ferromagnetic particles were reported by Mustafa et al. [21]. Rosali et al. [22] discussed the rotational effects on flow past an exponentially shrinking sheet and observed multiplicity of solutions in case of injection. Ahmad and Mustafa [23] performed a comparative study for revolving flow of nanofluids using two

different thermal conductivity models and convective conditions. Imtiaz et al. [24] explored the flow of carbon nanotubes between radially stretching disks by a homotopic approach.

In this thesis, we aim to explore the influences of binary chemical reaction with activation energy on rotating flow of Maxwell fluid over a stretchable surface. Coriolis and centrifugal effects attributed due to the fluid rotation are preserved in the mathematical model. Using similarity approach, self-similar solutions for velocity, temperature and concentration are developed. Graphical illustrations for velocity, temperature and concentration are presented to emphasize the physical effects of embedded parameters on the solutions. Numerical values of local Nusselt number and local Sherwood number for broad range of parameters are tabulated.

Chapter 2

Numerical solution for three dimensional flow of Maxwell fluid with non-linear thermal radiation

This chapter includes the review of an article by Mushtaq et al. [29]. The objective of this chapter is to investigate the effects of non-linear radiation on three-dimensional flow of upper-convected Maxwell (UCM) fluid over a surface which is being stretched in two lateral directions. The solutions for velocity and temperature are obtained numerically by using shooting method based on fifth-order Runge-Kutta algorithm. Graphs are presented to explore the physical behaviors of embedded parameters on the flow fluid.

2.1 Problem formulation

Consider a laminar flow of UCM fluid over a surface located in $xy-$plane (see Fig. 2.1). The surface is being stretched in $x-$ and $y-$directions with velocities $U_w(x) = ax$ and $V_w(y) = by$ respectively in which $a, b > 0$ are constants. The sheet is kept at constant temperature T_c and T_∞ denotes the temperature at the far field.
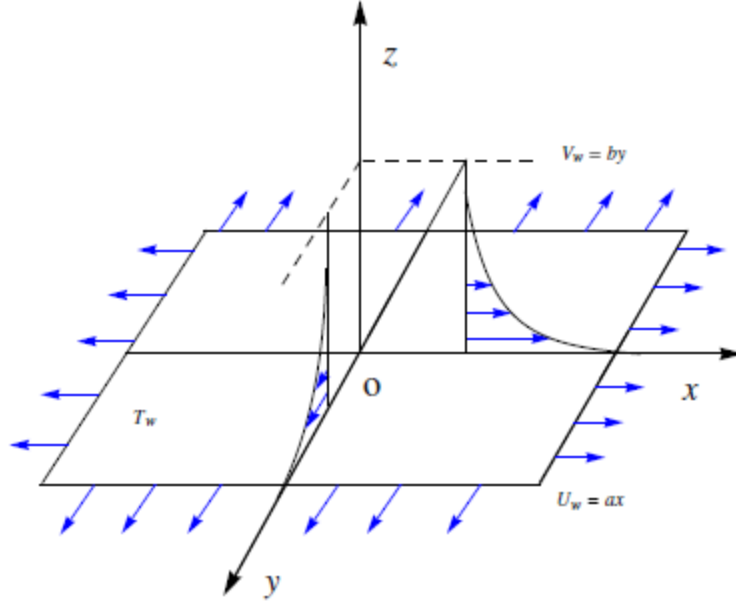
Fig. 2.1: A schematic diagram presenting the development of boundary layer

Based on scale analysis, the boundary layer approximations yield the following governing equations:

$$\frac{\partial u}{\partial x} + \frac{\partial v}{\partial y} + \frac{\partial w}{\partial z} = 0,$$ (2.1)

$$u\frac{\partial u}{\partial x} + v\frac{\partial u}{\partial y} + w\frac{\partial u}{\partial z} = \nu\frac{\partial^2 u}{\partial z^2} - \lambda_1\left(\begin{array}{c} u^2\dfrac{\partial^2 u}{\partial x^2} + v^2\dfrac{\partial^2 u}{\partial y^2} + w^2\dfrac{\partial^2 u}{\partial z^2} \\[2ex] +2uv\dfrac{\partial^2 u}{\partial x\partial y} + 2uw\dfrac{\partial^2 u}{\partial x\partial z} + 2vw\dfrac{\partial^2 u}{\partial y\partial z} \end{array}\right),$$ (2.2)

$$u\frac{\partial v}{\partial x} + v\frac{\partial v}{\partial y} + w\frac{\partial v}{\partial z} = \nu\frac{\partial^2 v}{\partial z^2} - \lambda_1\left(\begin{array}{c} u^2\dfrac{\partial^2 v}{\partial x^2} + v^2\dfrac{\partial^2 v}{\partial y^2} + w^2\dfrac{\partial^2 v}{\partial z^2} \\[2ex] +2uv\dfrac{\partial^2 v}{\partial x\partial y} + 2uw\dfrac{\partial^2 v}{\partial x\partial z} + 2vw\dfrac{\partial^2 v}{\partial y\partial z} \end{array}\right),$$ (2.3)

$$u\frac{\partial T}{\partial x} + v\frac{\partial T}{\partial y} + w\frac{\partial T}{\partial z} = \alpha\frac{\partial^2 T}{\partial z^2} - \frac{1}{\rho c_p}\frac{\partial q_r}{\partial z},$$ (2.4)

15

in which u, v and w are $x-, y-$ and $z-$ components of velocity respectively, λ_1 is the fluid relaxation time, v is the kinematic viscosity, α is the thermal diffusivity, ρ the fluid density, c_p is the specific heat, $q_r = -(4\sigma*/3k*)\partial T^4/\partial z$ is the Rosseland radiative heat flux in which $\sigma*$ is the Stefan-Boltzman constant and $k*$ is the mean absorption coefficient respectively.

The boundary conditions in the present problem are:

$$u = U_w(x) = ax, \quad v = V_w(y) = by, \quad w = 0, \quad T = T_w \qquad \text{at} \qquad z = 0,$$
$$u \to 0, \quad v \to 0, \quad T \to T_\infty \qquad \qquad \text{as} \qquad z \to \infty. \tag{2.5}$$

For similarity solution of Eq. (2.1)-(2.4) with the conditions (2.5), we introduce the non-dimensional distance η as

$$\eta = \sqrt{\frac{a}{v}} z, \tag{2.6}$$

with the following similarity variables

$$u = axf'(\eta), \quad v = ayg'(\eta), \quad w = -\sqrt{av}(f(\eta) + g(\eta)), \quad T = T_\infty + \Delta T\theta(\eta), \tag{2.7}$$

In which $\Delta T = T_w - T_\infty$ and prime denotes differentiation with respect to η.

In view of Eqs. (2.6) and (2.7), Eq. (2.1) is satisfied identically and Eqs. (2.2) - (2.4) are transformed into the following non-linear ordinary differential equations:

$$f''' - f'^2 + (f + g)f''^2 + K[2(f + g)ff'' - (f + g)^2 f'''] = 0, \tag{2.8}$$

$$g''' + g'^2 - (f + g)g'' + K[2(f + g)g'g'' - (f + g)^2 g'''] = 0, \tag{2.9}$$

$$\frac{1}{\Pr} \frac{d}{d\eta}\left[(1 + Rd(1 + (\theta_w - 1)\theta)^3)\theta'\right] + (f + g)\theta' = 0. \tag{2.10}$$

The transformed boundary conditions are

$$f = g = 0, \quad f' = 1, \quad g' = c, \quad \theta = 1 \text{ at } \eta = 0,$$
$$f' \to 0, \quad g' \to 0, \quad \theta \to 0 \text{ as } \eta \to \infty. \tag{2.11}$$

16

where $K = \lambda_1 a$ is the Deborah number, $\mathrm{Pr} = \nu / \alpha$ is the Prandtl number, $Rd = 16\sigma * T_\infty^3 / 3kk*$ is radiation parameter, $\theta_w = T_w / T_\infty$ is the temperature ratio parameter and $c = b / a$ denotes the ratio of stretching rate along $y-$direction to the stretching rate along the $x-$direction. It should be mentioned here that above problem corresponds to the case of two dimensional flow when $c = 0$ while axisymmetric flow is obtained by setting $c = 1$. We now define the local Nusselt number Nu_x as below:

$$Nu_x = \frac{xq_x}{k(T_w - T_\infty)},$$ (2.12)

where $q_w = -k(\partial T / \partial z)_{z=0} + (q_r)_{z=0}$ is the wall heat flux. Now putting the values of dimensionless quantities from Eq. (2.6) - (2.11), we get

$$\mathrm{Re}_x^{-1/2} Nu_x = -[1 + Rd\theta_w^3]\theta'(0),$$ (2.13)

where $\mathrm{Re}_x = U_w x / \nu$ is the local Reynolds number.

2.2 Numerical method

The solutions of Eq. (2.8) - (2.10) with the boundary conditions (2.11) have been developed by using shooting approach. For this purpose, we convert the equations into the system of first order equations by writing $x_1 = f, x_2 = f', x_3 = f'', x_4 = g, x_5 = g', x_6 = g'', x_7 = \theta, x_8 = \theta'$. We obtain the following:

$$
\begin{bmatrix} x_1' \\ x_2' \\ x_3' \\ x_4' \\ x_5' \\ x_6' \\ x_7' \\ x_8' \end{bmatrix} =
\begin{bmatrix}
x_2 \\[4pt]
x_3 \\[4pt]
\dfrac{-(x_1+x_4)x_3+\left(x_2\right)^2-2k(x_1+x_4)x_2x_3}{1-k(x_1+x_4)^2} \\[10pt]
x_5 \\[4pt]
x_6 \\[4pt]
\dfrac{-(x_1+x_4)x_6+\left(x_5\right)^2-2k(x_1+x_4)x_5x_6}{1-k(x_1+x_4)^2} \\[10pt]
x_8 \\[4pt]
-\dfrac{\Pr(x_1+x_4)x_8+3Rd(\theta_w-1)\left(x_8\right)^2-(\theta_w-1)^3(x_7)^2-2x_7(\theta_w-1)^2}{1+Rd\left(1+(\theta_w-1)x_7\right)^3}
\end{bmatrix}
\tag{2.14}
$$

with the following initial conditions

$$
\begin{bmatrix} x_1(0) \\ x_2(0) \\ x_3(0) \\ x_4(0) \\ x_5(0) \\ x_6(0) \\ x_7(0) \\ x_8(0) \end{bmatrix} =
\begin{bmatrix} 0 \\ 1 \\ u_1 \\ 0 \\ c \\ u_2 \\ 1 \\ u_3 \end{bmatrix},
\tag{2.15}
$$

where $\left[u_1, u_2, u_3\right] = \left[f''(0), g''(0), \theta'(0)\right]$. The system given in Eq. (2.14) is integrated via fifth order Runge-Kutta integration scheme. Newton's method is employed to estimate the unknown slopes $f''(0)$, $g''(0)$ and $\theta'(0)$. All the computations are done successfully in MATLAB.

2.3 Results and discussion

To validate the given simulations we compared the numerical results of $f''(0)$, $g''(0)$ and $\theta'(0)$ with Lie and Andersson [25] in a limiting sense. The results look like to be nearly identical in all the cases as can be understood through Table 2.1.

c	Liu and Andersson [25]			Present		
	$-f''(0)$	$-g''(0)$	$-\theta'(0)$	$-f''(0)$	$-g''(0)$	$-\theta'(0)$
0	1	0	-	1	0	0.5819785
0.25	1.048813	0.194565	0.665933	1.048811	0.1945639	0.6659264
0.50	1.093096	0.465206	0.735334	1.093094	0.4652047	0.7353326
0.75	1.134486	0.794619	0.796472	1.134486	0.7946183	0.7964708
1	1.173721	1.173721	-	1.173721	1.1737210	0.8519916

Table 2.1: Comparison of present results with Liu and Andersson [25] when $K = 0,$ $\Pr = 1,$ and $Rd = 0.$

Figs. 2.2 - 2.8 are prepared to illustrate the behavior of embedded flow parameters on the velocity and temperature profiles.
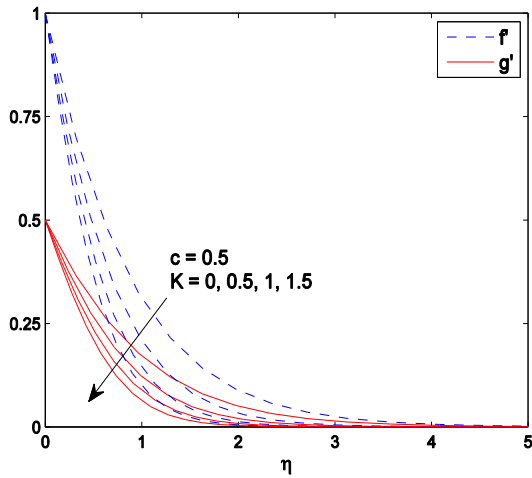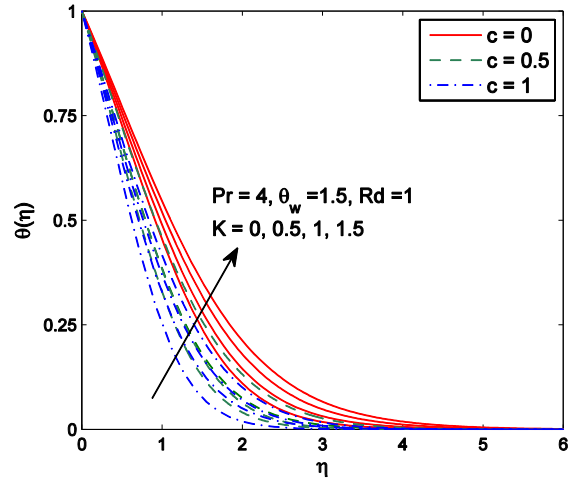

Fig. 2.2: Effect of K on $f'(\eta)$ and $g'(\eta)$.

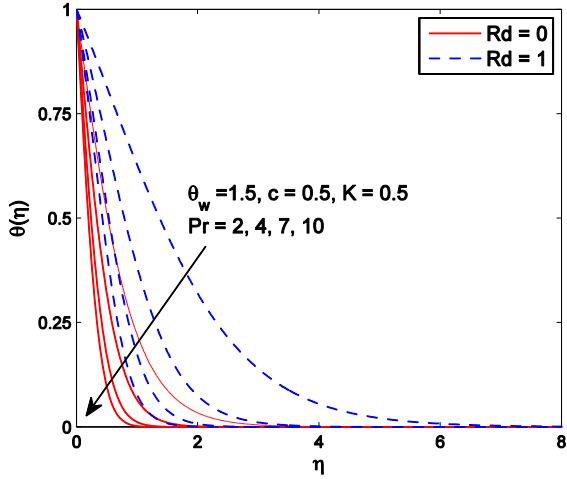Fig. 2.3: Effect of K and c on $\theta(\eta)$.

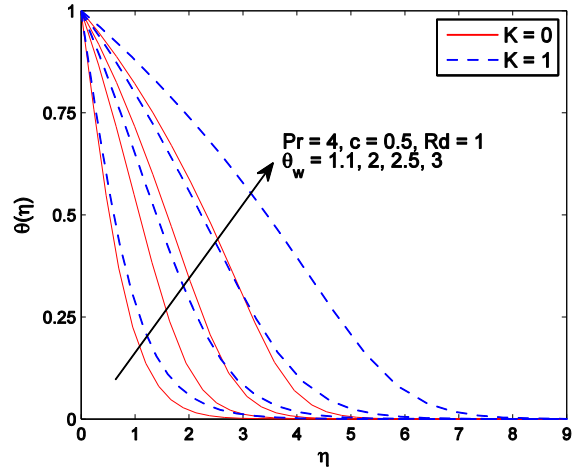Fig. 2.4: Effect of $\Pr$ and Rd on $\theta(\eta)$.

Fig. 2.5: Effect of θ_w and K on $\theta(\eta)$.
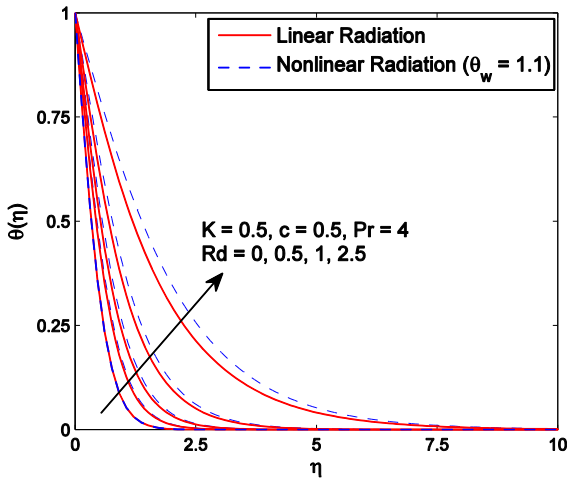

Fig. 2.6: Effect of Rd on $\theta(\eta)$ when $\theta_w = 1.1$.
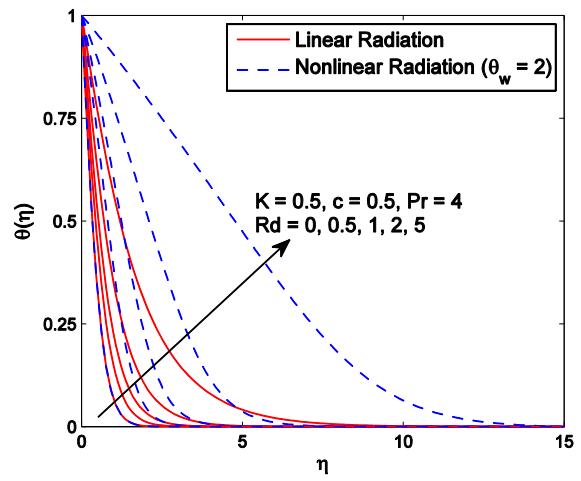

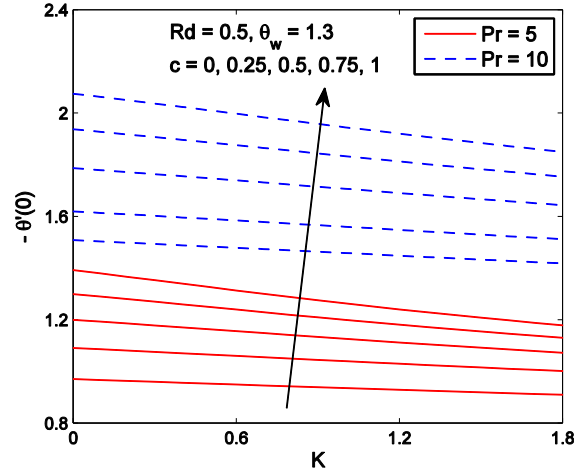Fig. 2.7: Effect of Rd on $\theta(\eta)$ when $\theta_w = 2$.

Fig. 2.8: Effect of K and c on $-\theta'(0)$ for $\Pr = 5$ and $\Pr = 10$.

The effect of Deborah number K on the velocity profile is shown in Fig. 2.2. An increase in K corresponds to an increase in the fluid relaxation time. Smaller fluid relaxation time represents viscous fluids. When relaxation time increases, the fluid tends to behave like elastically solid substance. The boundary layer thins when K is increased. Also the change in velocity fields f' and g' is greater in three-dimensional flow when compared with axisymmetric and two dimensional flows. Fig. 2.3 shows the change in temperature θ when Deborah number K is varied. It is found that the temperature θ rises as the fluid relaxation time increases. It means that elastic effects enhance the temperature of viscoelastic fluids. Fig. 2.4 displays that the thermal boundary layer thins with the increase in Prandtl number $\Pr$. The reason is that increasing $\Pr$ reduces the thermal diffusivity which restricts the penetration depth of temperature. Fig. 2.5 exhibits the effect of temperature ratio parameter θ_w on the temperature distribution. An increase in θ_w results in the thickening of thermal boundary layer. This effect is explained as follow. Eq. (2.4) shows that thermal diffusivity is the sum of classical thermal diffusivity α and the thermal diffusivity due non-linear radiative heat flux. Thus θ_w being the coefficient of later term, supports the thickness of boundary layer. It can also be observed that a special S-shaped profile is obtained when θ_w is increased which is an indicator of inflection point for temperature distribution. That is for sufficiently large wall to ambient temperature ratio, the temperature gradient approaches to zero. The influence of radiation parameter Rd on temperature profile is

shown in Fig. 2.6 for both linear and non-linear cases. It can be analyzed that both profiles coincide only for small values of Rd while for large values of Rd, they disperse continuously. Also as the temperature ratio rises from $\theta_w = 1.1$ to $\theta_w = 2$, the profiles in case of non-linear radiation move away from the corresponding profiles of linear radiation case. Fig. 2.7 points to the conclusion that only for θ_w approximately equal to unity and Rd is sufficiently small (say $Rd < 0.1$), the result for linear and non-linear radiation would become identical. Fig. 2.8 represents the effects of $\Pr$ on the local Nusselt number at different values of K. It shows that magnitude of $\theta'(0)$ has inverse and non-linear relationship with Deborah number K. The reason is that fluids with large Prandtl number exhibit strong convection compared to pure conduction. Also from Fig. 2.4 we've already seen that large value of $\Pr$ makes the profile steeper. Thus the heat transfer rate from the surface grows as $\Pr$ increases.

Table 2.2 contains the values of wall slope of temperature $\theta'(0)$ for different values of $K, c, \Pr$ and Rd. The heat transfer rate reduces nearly 6% in the absence of thermal radiation with K varies when $K = 0$ from $K = 1.5$ with $\Pr = 7$ and $c = 0.5$. This reduction is increased to about 10% in case of non-linear radiation with $\theta_w = 1.5$.

K	c	Pr	$Rd = 0$	$Rd = 1$		
				Linear radiation	Non-linear radiation	
					$\theta_w = 1.1$	$\theta_w = 1.5$
1	0.5	2	1.01695	0.61177	0.53932	0.31686
		4	1.60165	1.01695	0.90348	0.55107
		7	2.24393	1. 47271	1.31435	0.82083
		10	2.75508	1. 83692	1.64284	1.03739
1	0	7	1.82603	1. 20254	1.07372	0.67255
	0.3		2.09403	1. 37824	1.23051	0.77013
	0.6		2.31293	1. 51544	1.35219	0.84341
	1		2.55918	1. 66440	1.48361	0.92038
0	0.5	7	2.35436	1. 59321	1.42760	0.91088
0.5			2.29665	1. 53021	1.36840	0.86380
1			2.24393	1. 47271	1.31435	0.82083
1.5			2.19501	1.41998	1.26482	0.78170

Table 2.2: Numerical result of wall temperature gradient $-\theta'(0)$ for different values of K, c, Pr and Rd.

23

Chapter 3

Rotating flow of Maxwell fluid over a stretchable surface with a binary chemical reaction and activation energy

The objective of this chapter is to investigate the effects of a binary chemical reaction and activation energy on three-dimensional flow of upper-convected Maxwell (UCM) fluid over a surface which is being stretched in one directions. The solutions for velocity, temperature and concentration are obtained numerically by using shooting method based on fifth-order Runge-Kutta algorithm. Graphs are presented to explore the physical behaviors of embedded parameters on the flow fluid.

3.1   Problem formulation

Consider a three-dimensional flow of an incompressible Maxwell fluid over an elastic surface located in the $xy-$plane. The fluid resides in the space $z \geq 0$. The surface is stretched in the $x-$ direction with the linearly varying velocity of the form $u_w(x) = ax$ which induces flow in the neighboring layers of the fluid. Let Ω be the constant angular velocity of the rotating fluid. The surface is kept at constant temperature T_w and solute concentration at the surface is denoted by C_w. Let T_∞ and C_∞ be the ambient values of temperature and solute concentration respectively. Physical sketch of the problem is shown in Fig. 1. Governing equations in the presence of species chemical reaction with Arrhenius activation energy are expressed below:
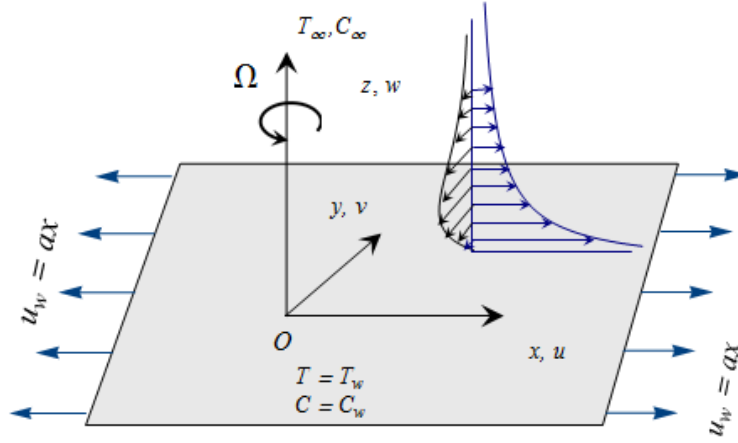
Fig. 3.1: Physical configuration and coordinate system.

$$\nabla.\mathbf{V} = 0, \tag{3.1}$$

$$\rho\left[(\mathbf{V}.\nabla)\mathbf{V} + (\mathbf{\Omega}\times(\mathbf{\Omega}\times\mathbf{r})) + (2\mathbf{\Omega}\times\mathbf{V})\right] = -\nabla p + \nabla.\mathbf{S}, \tag{3.2}$$

$$\rho c_p(\mathbf{V}.\nabla T) = k\nabla^2 T, \tag{3.3}$$

$$(\mathbf{V}.\nabla C) = D\nabla^2 C - k_r^2\left(\frac{T}{T_\infty}\right)^n e^{-\frac{E_a}{\kappa T}}(C - C_\infty), \tag{3.4}$$

where k is the thermal conductivity, D the solute diffusivity, ρ the fluid density, c_p the specific heat and $\mathbf{\Omega} = [0,0,\Omega]$ the angular velocity vector. The term $\mathbf{\Omega}\times(\mathbf{\Omega}\times\mathbf{r}) = -\nabla(\Omega^2 r^2/2)$ represents the centrifugal force which is being balanced by the pressure gradient $-\nabla p$. The term $k_r^2(T/T_\infty)^n e^{-\frac{E_a}{kT}}$ is the modified Arrhenius function [11] in which $\kappa = 8.61\times10^{-5} eV/K$ is the Boltzmann constant, k_r^2 the reaction rate and n the fitted rate constant generally lies in $-1 < n < 1$. In Eq. (2), $\mathbf{S}$ is the extra stress tensor for upper-convected Maxwell fluid which satisfies the following:

25

$$\mathbf{S} + \lambda_1 \frac{D\mathbf{S}}{Dt} = \mu \mathbf{A}_1,$$

in which λ_1 is the fluid relaxation time, $\mathbf{A}_1 = (\nabla \mathbf{V}) + (\nabla \mathbf{V})^t$ the first Rivlin-Ericksen tensor and D/Dt the upper-convected time derivative. Invoking the conventional boundary layer approximations, Eqs. (3.1) - (3.4) can be expressed in component forms as below:

$$\frac{\partial u}{\partial x} + \frac{\partial v}{\partial y} + \frac{\partial w}{\partial z} = 0, \tag{3.5}$$

$$u\frac{\partial u}{\partial x} + v\frac{\partial u}{\partial y} + w\frac{\partial u}{\partial z} - 2\Omega v = v\left(\frac{\partial^2 u}{\partial z^2}\right) - \lambda_1 \begin{bmatrix} u^2\dfrac{\partial^2 u}{\partial x^2} + v^2\dfrac{\partial^2 u}{\partial y^2} + w^2\dfrac{\partial^2 u}{\partial z^2} \\[2mm] +2uv\dfrac{\partial^2 u}{\partial x \partial y} + 2vw\dfrac{\partial^2 u}{\partial y \partial z} + 2uw\dfrac{\partial^2 u}{\partial x \partial z} \\[2mm] -2\Omega\left(u\dfrac{\partial v}{\partial x} + v\dfrac{\partial v}{\partial y} + w\dfrac{\partial v}{\partial z}\right) + 2\Omega\left(v\dfrac{\partial u}{\partial x} - u\dfrac{\partial u}{\partial y}\right) \end{bmatrix}, \tag{3.6}$$

$$u\frac{\partial v}{\partial x} + v\frac{\partial v}{\partial y} + w\frac{\partial v}{\partial z} + 2\Omega u = v\left(\frac{\partial^2 v}{\partial z^2}\right) - \lambda_1 \begin{bmatrix} u^2\dfrac{\partial^2 v}{\partial x^2} + v^2\dfrac{\partial^2 v}{\partial y^2} + w^2\dfrac{\partial^2 v}{\partial z^2} \\[2mm] +2uv\dfrac{\partial^2 v}{\partial x \partial y} + 2vw\dfrac{\partial^2 v}{\partial y \partial z} + 2uw\dfrac{\partial^2 v}{\partial x \partial z} \\[2mm] +2\Omega\left(u\dfrac{\partial u}{\partial x} + v\dfrac{\partial u}{\partial y} + w\dfrac{\partial u}{\partial z}\right) + 2\Omega\left(v\dfrac{\partial v}{\partial x} - u\dfrac{\partial v}{\partial y}\right) \end{bmatrix}, \tag{3.7}$$

$$u\frac{\partial T}{\partial x} + v\frac{\partial T}{\partial y} + w\frac{\partial T}{\partial z} = \alpha \frac{\partial^2 T}{\partial z^2}, \tag{3.8}$$

$$u\frac{\partial C}{\partial x} + v\frac{\partial C}{\partial y} + w\frac{\partial C}{\partial z} = D\frac{\partial^2 C}{\partial z^2} - k_r^2\left(\frac{T}{T_\infty}\right)^n e^{-\frac{E_a}{kT}}(C - C_\infty). \tag{3.9}$$

The boundary conditions in the present problem are:

$$\begin{aligned} u &= ax, \quad v = 0, \quad w = 0, \quad T = T_w, \quad C = C_w \quad \text{at } z = 0, \\ u &\to 0, \quad v \to 0, \quad T \to T_\infty, \quad C \to C_\infty \quad \text{as } z \to \infty. \end{aligned} \tag{3.10}$$

26

We introduce the following set of similarity variables involving dimensionless vertical distance η as

$$\eta = \sqrt{\frac{a}{v}}z, \quad u = axf'(\eta), \quad v = axg(\eta), \quad w = -\sqrt{av}f(\eta), \quad \theta = \frac{T - T_\infty}{T_w - T_\infty}, \quad \phi = \frac{C - C_\infty}{C_w - C_\infty}, \tag{3.11}$$

Eq. (3.5) is identically satisfied and Eqs. (3.6) - (3.9) convert into the following ordinary differential equations:

$$f''' + ff'' - f'^2 + 2\lambda(g - \beta fg') + \beta[2fff'' - f^2f'''] = 0, \tag{3.12}$$

$$g'' + fg' - gf' - 2\lambda\left[f' + \beta\left(f'^2 - ff'' + g^2\right)\right] + \beta[2ff'g' - f^2g''] = 0, \tag{3.13}$$

$$\frac{1}{\text{Pr}}\theta'' + f\theta' = 0, \tag{3.14}$$

$$\frac{1}{Sc}\phi'' + f\phi' - \sigma[1 + \delta\theta]^n \exp\left[-\frac{E}{1 + \delta\theta}\right]\phi = 0, \tag{3.15}$$

subject to the transformed conditions

$$\text{at } \eta = 0: f = g = 0, \quad f' = 1, \quad \theta = \phi = 1,$$
$$\text{as } \eta \to \infty: f' \to 0, \quad g \to 0, \quad \theta \to 0, \quad \phi \to 0. \tag{3.16}$$

where $\lambda = \Omega/a$ is the rotation parameter, $\beta = \lambda_1 a$ the Deborah number, $Pr = \mu c_p / k$ the Prandlt number, $Sc = v/D$ the Schmidt number, $E = E_a/(\kappa T_\infty)$ the non-dimensional activation energy, $\delta = (T_w - T_\infty)/T_\infty$ the temperature difference parameter, $\sigma = k_r^2/a$ the dimensionless reaction rate. Fourier law can be used to define local Nusselt number Nu_x and Fick's law can be employed to define local Sherwood number Sh_x. These are as follows:

$$Nu_x = \frac{xq_w}{k(T_w - T_\infty)}, \quad Sh_x = \frac{xj_w}{D(C_w - C_\infty)}, \tag{3.17}$$

where q_w is the wall heat flux and j_w is the wall mass flux given by

$$q_w = -k \frac{\partial T}{\partial z}\bigg|_{z=0}, \quad j_w = -D \frac{\partial C}{\partial z}\bigg|_{z=0}. \tag{3.18}$$

Now using Eq. (3.11) and Eq. (3.18), Eq. (3.17) becomes

$$\frac{Nu_x}{\sqrt{Re_x}} = -\theta'(0), \frac{Sh_x}{\sqrt{Re_x}} = -\phi'(0), \tag{3.19}$$

where $Re_x = ax^2/v$ is the local Reynolds number.

3.2 Numerical method

Here we deal with the numerical solutions of Eqs. (3.12) - (3.15) with the conditions (3.16) by conventional shooting approach. We convert Eqs. (3.12) - (3.16) into a system of first order equations by writing $f = x_1, f' = x_2, f'' = x_3, g = x_4, g' = x_5, \theta = x_6, \theta' = x_7, \phi = x_8, \phi' = x_9.$ We obtain the following:

$$\begin{bmatrix} x_1' \\ x_2' \\ x_3' \\ x_4' \\ x_5' \\ x_6' \\ x_7' \\ x_8' \\ x_9' \end{bmatrix} = \begin{bmatrix} x_2 \\ x_3 \\ \left(x_2^2 - x_1 x_3 - 2\lambda\left(x_4 - \beta x_1 x_5\right) - 2\beta x_1 x_2 x_3\right)/\left(1 - \beta x_1^2/2\right) \\ x_5 \\ \left(x_2 x_4 - x_1 x_5 + 2\lambda\left(x_2 + \beta\left(x_2^2 - x_1 x_3 + x_4^2\right)\right) - 2\beta x_1 x_2 x_5\right)/\left(1 - \beta x_1^2/2\right) \\ x_7 \\ -\Pr x_1 x_7 \\ x_9 \\ Sc\left(\sigma\left[1 + \delta x_6\right]^n \exp\left[-E/\left(1 + \delta x_6\right)\right]x_8 - x_1 x_9\right) \end{bmatrix}, \tag{3.20}$$

with the following initial conditions

$$
\begin{bmatrix}
x_1(0) \\
x_2(0) \\
x_3(0) \\
x_4(0) \\
x_5(0) \\
x_6(0) \\
x_7(0) \\
x_8(0) \\
x_9(0)
\end{bmatrix}
=
\begin{bmatrix}
0 \\
1 \\
u_1 \\
0 \\
u_2 \\
1 \\
u_3 \\
1 \\
u_4
\end{bmatrix},
\tag{3.21}
$$

where $[u_1, u_2, u_3, u_4] = [f''(0), g'(0), \theta'(0), \phi'(0)]$. The first order system (3.20) can be integrated numerically through fifth-order Runge-Kutta method by assigning appropriate values to u_1, u_2, u_3 and u_4. Newton-Raphson method is implemented to iteratively estimate these values. The whole process is repeated at different $\eta_{\max}$ say $\eta = 10, 11, 12, 13$ until the solutions exponentially tend to free stream conditions with specified tolerance say 10^{-5}. The obtained solutions are found to be consistent with those from the MATLAB built in routine *bvp4c*.

3.3 Results and discussion

To validate our results we have made table 3.1 for different values of β when rotating parameter $\lambda = 0$. The values of $-f''(0)$ are found in great agreement with that of Abel et al. [26] and Megahed [27].

β	Abel et al. [26]	Megahed [27]	Abbasi et al. [28]	Present results
0.0	0.999962	0.999978	1.000000	1.000000
0.2	1.051948	1.051945	1.05189	1.051887
0.4	1.101850	1.101848	1.10190	1.101898
0.6	1.150163	1.150160	1.15014	1.150128
0.8	1.196692	1.196690	1.19671	1.196708
1.2	1.285257	1.285253	1.28536	1.285361
1.6	1.368641	1.368641	1.36873	1.368756
2.0	1.447617	1.447616	1.44781	1.447648

Table 3.1: Comparison with $-f''(0)$ obtained by Abel et al. [26] and Megahed [27] for different values of β when rotating parameter $\lambda = 0$.

In this section, our focus is to analyze the role of embedded parameters on the velocity, temperature and concentration profiles. For that Figs. 3.2 – 3.15 are prepared.
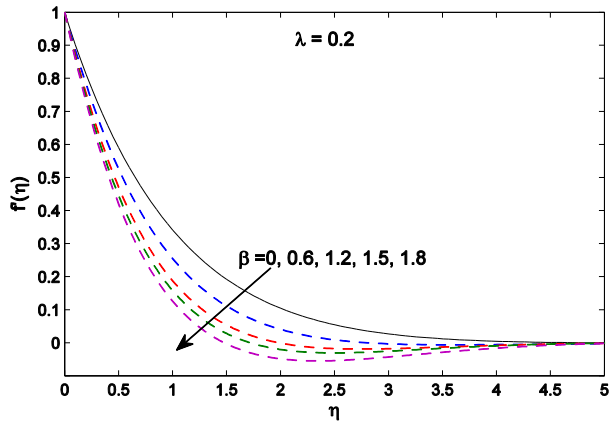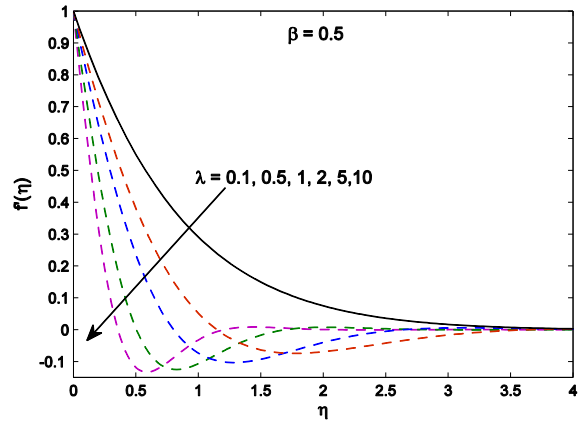

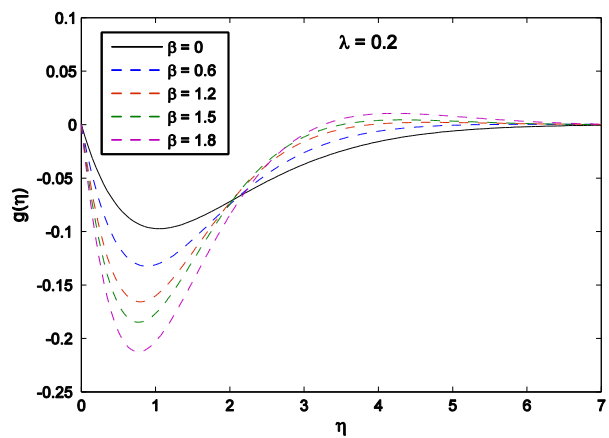Fig. 3.2: Effect of β on $f'(\eta)$.

Fig. 3.3: Effect of λ on $f'(\eta)$.
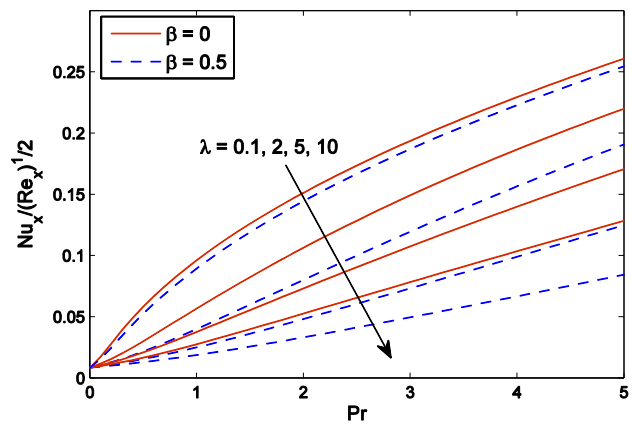

Fig. 3.4: Effect of β on $g(\eta)$.

Fig. 3.5: Effect of Pr and λ on $Nu_x / \sqrt{Re_x}$ for $\beta = 0$ and $\beta = 0.5$.
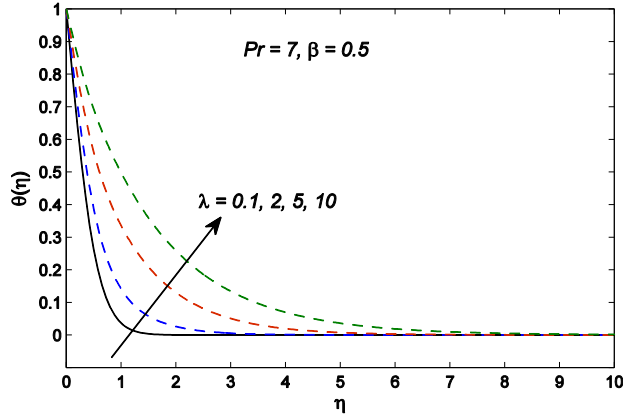
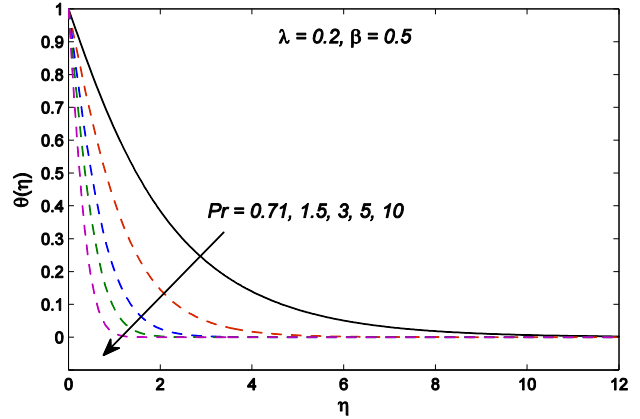Fig. 3.6: Effect of λ on $\theta(\eta)$.
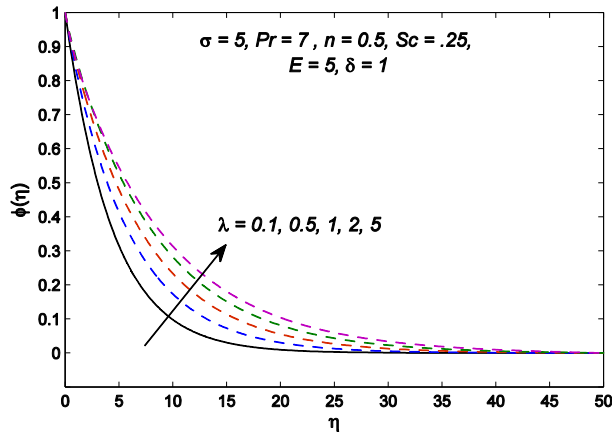

Fig. 3.7: Effect of Pr on $\theta(\eta)$.

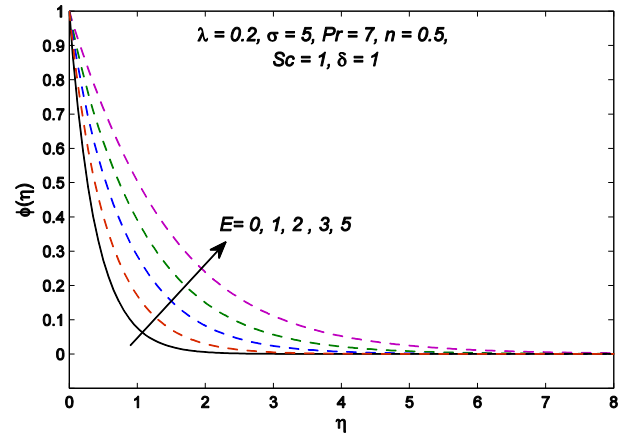

Fig. 3.8: Effect of λ on $\phi(\eta)$.
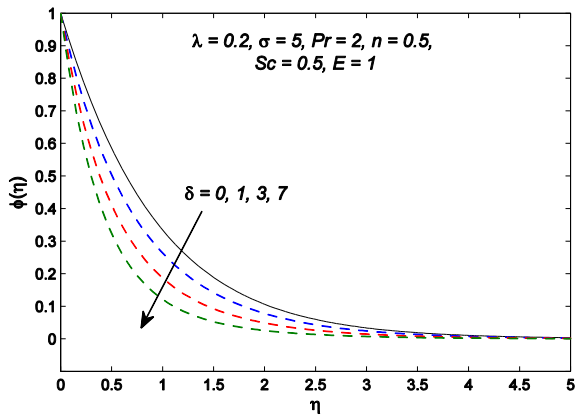

Fig. 3.9: Effect of E on $\phi(\eta)$.

Fig. 3.10: Effect of δ on $\phi(\eta)$.
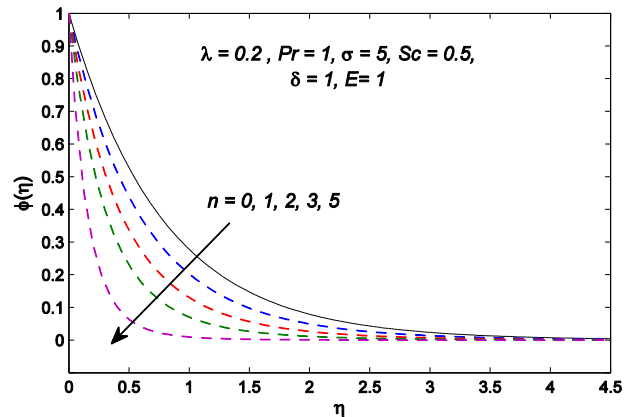

Fig. 3.11: Effect of n on $\phi(\eta)$.

Fig. 3.12: Effect of σ on $\phi(\eta)$.
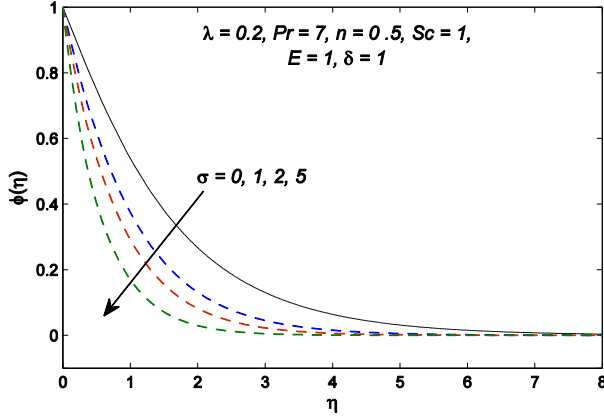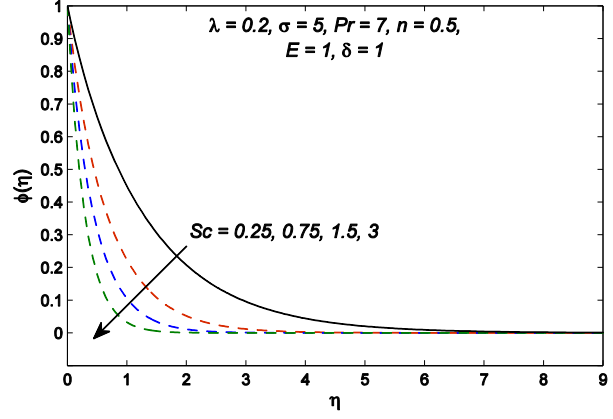

Fig. 3.13: Effect of Sc on $\phi(\eta)$.
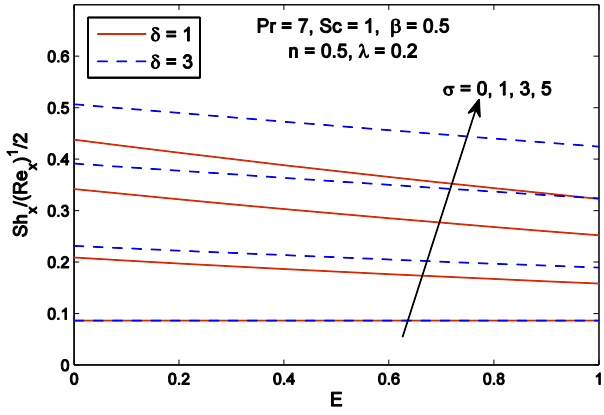
Fig. 3.14: Effect of E and σ on $Sh_x / \sqrt{Re_x}$ for $\delta = 1$ and $\delta = 3$.
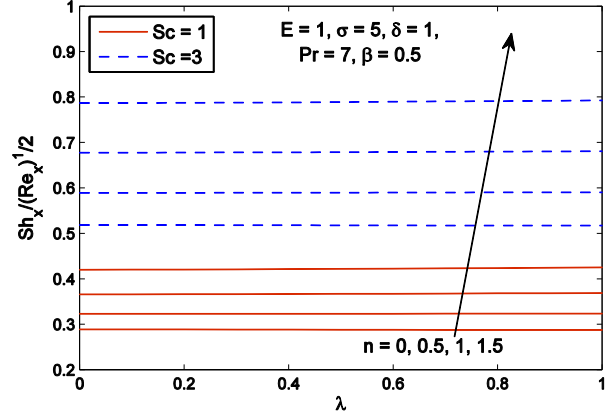
Fig. 3.15: Effect of λ and n on $Sh_x / \sqrt{Re_x}$ for $Sc = 1$ and $Sc = 3$.

Fig. 3.2 preserves the influence of Deborah number β on the velocity field f' when $\lambda = 0.2$. The profiles indicate a decreasing trend in f' for increasing values of β. It means that fluid motion in the $x-$direction is opposed by the viscoelastic effects. For larger values of β, the profiles of f' tend to zero at smaller distances above the sheet. In smaller Deborah number fluid, viscous effect is dominant compared to the elastic effect whereas the fluid tends to behave as elastically solid material when Deborah number enlarges. In Fig. 3.3, the influence of rotation parameter λ on the velocity in $x-$direction is observed. The rotational effects tend to slow down the fluid motion in the $x-$direction. For smaller λ, the decrease in velocity field f' with η is monotonic while an interesting oscillatory behavior in f' is observed for large λ which is due to the rotational effects. Fig. 3.4 shows the profiles of g for various values of Deborah

number β with $\lambda = 0.2$. The negative value of g reveals that flow is solely in the negative $y-$ direction. For larger value of λ, the oscillations in the profile of g analogous to those of f' are observed.

Fig. 3.5 is presented to analyze the influence of rotation on the local Nusselt number which determines the heat transfer rate from the sheet. It is observed that the local Nusselt number approaches zero for vanishing Prandtl number Pr and it increases upon increasing Pr. It is also clear that local Nusselt number has inverse relationship with λ. It means that heat transfer rate reduces when fluid is subjected to larger rotation rate. In Fig. 3.6 we have plotted temperature field θ for different values of parameter λ. Temperature θ increases and thermal boundary layer becomes thicker upon increasing the parameter λ. Physically it is attributed to the fact that larger rotation parameter λ gives larger kinetic energy to the fluid which enhances its temperature. Fig. 3.7 shows the relation between Prandtl number Pr and temperature θ. Larger Prandtl number implies weaker thermal diffusivity that leads to thinner penetration depth of temperature.

In Fig. 3.8, the effects of rotation parameter λ on the concentration profile $\phi(\eta)$ have been shown. It depicts that concentration boundary layer thickness grows when angular velocity Ω is increased. Concentration profiles for various values of dimensionless activation energy E have been plotted in Fig. 3,9. It reveals that increasing the dimensionless activation energy causes the thickening of the concentration boundary layer. This is because low temperature and high activation energy leads to smaller reaction rate constant and thus slow down the chemical reaction. Consequently, the concentration of the solute increases. Fig. 3.10 shows the variation in solute concentration with the variation in temperature difference parameter δ. It is observed that solute concentration ϕ is a decreasing function of δ. This implies that concentration boundary layer thickness increases when difference between wall and ambient temperature enlarges. Figs. 3.11 and 3.12 are prepared to observe the influence of fitted rate constant n and reaction rate σ on solute concentration ϕ respectively. It can be observed that an increase in either n or σ results in an increase in the factor $\sigma(1+\delta\theta)^n \exp(-E/1+\delta\theta)$. This eventually favors the destructive chemical reaction due to which concentration rises. The reduction in ϕ is accompanied with larger concentration gradient at the wall. The effects of Schimdt number Sc

on concentration profile can be noticed from Fig. 3.13. It illustrates the thinning of concentration boundary layer when Sc is increased. Physically, an increase in Schmidt number Sc corresponds to lower solute diffusivity which results in shorter penetration depth of concentration.

Plots of local Sherwood number $\mathrm{Re}_x^{-1/2} Sh_x$ versus activation energy E at different values of reaction rate constant σ have been included in Fig. 3.14. There is a decrease in $\mathrm{Re}_x^{-1/2} Sh_x$ as E increases and this decrease is pronounced when larger values of σ are employed. It means that mass flux from the sheet is smaller when chemical reaction requires larger activation energy. Fluid rotation rate seem to have a mild influence on the wall mass flux for any prescribed values of n and Sc (see Fig. 3.15). The magnitude of $\mathrm{Re}_x^{-1/2} Sh_x$ is increased when Schmidt number Sc is varied from $Sc = 1$ to $Sc = 3$.

Tables 3.2 and 3.3 are presented to observe the trends in wall heat and mass transfer rates with the variation in embedded parameters.

Table 3.2 shows that magnitude of local Nusselt number $\mathrm{Re}_x^{-1/2} Nu_x$ increases as the rotation parameter λ and Deborah number β increase while it significantly grows as Prandtl number Pr increases. In other words, fluid rotation and viscoelasticity have adverse impact on the cooling process of the sheet. Table 3.3 indicates a sharp growth in local Sherwood number $\mathrm{Re}_x^{-1/2} Sh_x$ when either Schmidt number Sc or reaction rate constant σ is incremented. Schmidt number compares the momentum diffusion to mass diffusion. Thus concentration boundary layer becomes thinner and mass transfer rate augments when Sc increases.

λ	β	Pr	$-\theta'(0)$
0.2	0.5	1	0.51903
1.0			0.34237
1.5			0.27827
2.0			0.23746
0.2	0.2	1	0.54670
	0.4		0.52809
	0.6		0.51009
	0.8		0.49255
0.2	0.5	2	0.85109
		5	1.51553
		7	1.84540
		10	2.26033

Table 3.2: Numerical values of local Nusselt number $-\theta'(0)$ for various values of λ, Pr and β.

Sc	λ	E	σ	$-\phi'(0)$
1	0.2	1	1	0.95064
3				1.80760
5				2.40990
8				3.12064
1	0.1	1	1	0.95576
	1			0.90663
	2			0.88791
	3			0.88577
1	0.2	2	1	0.75333
		4		0.58015
		6		0.53528
		8		0.52368
0.2	0.2	1	1.5	0.43149
			2.0	0.49336
			2.5	0.54928
			3	0.60083

Table 3.3: Numerical values of local Sherwood number $-\phi'(0)$ for different values of Sc, λ, E

and σ.

Chapter 4

Conclusions

Heat transfer involving non-linear radiative flux on the flow of Maxwell fluid over a bidirectional stretching surface and heat and mass transfer involving Arrhenius activation energy and binary chemical reaction on the flow of Maxwell fluid in a rotating frame is presented and analyzed. The major points of this work are as follows:

1. Boundary layer of Newtonian fluids is thicker than the boundary layer of Maxwell fluids.

2. In non-linear radiation, thermal boundary layer is controlled by variable thermal diffusivity of the form $(\alpha + 16\sigma^* T^3 / 3\rho c_p k^*)$.

3. Temperature profile becomes S-shaped in pattern for sufficiently large values of θ_w .

4. Velocities in the x- and y-directions decrease as fluid relaxation time λ_1 increases. Also, wall heat flux reduces upon increasing the fluid relaxation time λ_1 .

5. Hydrodynamic boundary layer thins when rotation parameter λ is incremented. An oscillatory behavior in both x- and y-components of velocity is observed when rotation parameter λ is sufficiently large.

6. The vertical component of velocity at far field decreases when either Deborah number β or rotation parameter λ is increased.

7. Thermal boundary layer significantly grows when fluid rotates at larger angular velocity. This growth is accompanied with a reduction in wall slope of temperature and eventually the local Nusselt number.

8. Solute concentration ϕ increases and wall mass flux reduces when larger rotation parameter λ is employed.

9. Activation energy E enhances the solute concentration and reduces wall mass flux. This reduction grows further when difference between wall and ambient temperatures is increased.

10. Solute concentration ϕ reduces when reaction rate constant σ enlarges. Concentration ϕ is also inversely proportional to the temperature differences.

11. Schmidt number Sc decreases the solute concentration and supports the mass transfer rate from the wall.

Bibliography

1. A. J. Chamkha, A. M. Rashad and H. Al-Mudhaf, Heat and mass transfer from truncated cones with variable wall temperature and concentration in the presence of chemical reaction effects, Int. J. Numer. Meth. Heat &Fluid Flow 22 (2012) 357-376.

2. B. Mallikarjuna, A. M. Rashad, A. J. Chamkha and S. H. Raju, Chemical reaction effects on MHD convective heat and mass transfer flow past a rotating vertical cone embedded in a variable porosity regime, Afrika Matematika, 27 (2015) 645-665.

3. C. Zhang, L. Zheng, X. Zhang and G. Chen, MHD flow and radiation heat transfer of nanofluids in porous media with variable surface heat flux and chemical reaction, Appl. Math. Model. 39 (2015) 165-181.

4. N. Khan, T. Mahmood, M. Sajid and M. S. Hashmi, Heat and mass transfer on MHD mixed convection axisymmetric chemically reactive flow of Maxwell fluid driven by exothermal and isothermal stretching disks, Int. J. Heat Mass Transf. 92 (2016) 1090-1105.

5. F. Mabood, S. Shateyi, M. M. Rashidi, E. Momoniat and N. Freidoonimehr, MHD stagnation point flow heat and mass transfer of nanofluids in porous medium with radiation, viscous dissipation and chemical reaction, Adv. Pow. Tech. 27 (2016) 742-749.

6. S. Rawat, S. Kapoor and R. Bhargava, MHD flow heat and mass transfer of micropolar fluid over a nonlinear stretching sheet with variable micro inertia density, heat flux and chemical reaction in a non-darcy porous medium, J. Appl. Fluid Mech. 9 (2016) 321-331.

7. Bestman, Natural convection boundary layer with suction and mass transfer in a porous medium, Int. J. Engg. Res. 14 (1990) 389-396. doi: 10.1002/er.4440140403.

8. O. D. Makinde, P. O. Olanrewaju and W. M. Charles, Unsteady convection with chemical reaction and radiative heat transfer past a flat porous plate moving through a binary mixture, Africka Matematika 22 (2011) 65-78. doi: 10.1007/s13370-011-0008-z.

9. K. A. Maleque, Effects of binary chemical reaction and activation energy on MHD boundary layer heat and mass transfer flow with viscous dissipation and heat generation/absorption, ISRN Thermodyn. (2013) Article ID 284637 doi: 10.1155/2013/284637.

10. K. A. Maleque, Effects of exothermic/endothermic chemical reactions with Arrhenius activation energy on MHD free convection and mass transfer flow in presence of thermal radiation, J. Thermodyn. (2013). Article ID 692516, doi:10.1155/2013/692516.

11. F. G. Awad , S. Motsa and M. Khumalo, Heat and mass transfer in unsteady rotating fluid flow with binary chemical reaction and activation energy (2014). PLoS ONE 9(9): e107622. doi:10.1371/journal.pone.0107622.

12. C. Y. Wang, Stretching a surface in a rotating fluid, J. Appl. Math. Phys. (ZAMP) 39 (1988) 177-185.

13. H. S. Takhar, A. J. Chamkha and G. Nath, Flow and heat transfer on a stretching surface in a rotating fluid with a magnetic field, Int. J. Therm. Sci. 42 (2003) 23-31.

14. R. Nazar, N. Amin and I. Pop,Unsteady boundary layer flow due to a stretching surface in a rotating fluid, Mech. Res. Comm. 31 (2004) 121-128.

15. M. Kumari, T. Grosan and I. Pop, Rotating flows of power-law fluids over a stretching surface, Technische Mechanik 1 (2006) 11-19.

16. K. Zaimi, A. Ishak and I. Pop, Stretching surface in rotating viscoelastic fluid, Appl. Math. Mech. 34 (2013) 945-952.

17. T. Javed, M. Sajid, Z. Abbas and N. Ali, Non-similar Solution for rotating flow over an exponentially stretching surface, Int. J. Numer. Meth. Heat Fluid Flow 21 (2011) 903-908.

18. M. Mustafa, Cattaneo-Christov heat flux model for rotating flow and heat transfer of upper-convected Maxwell fluid, AIP Advances 5, 047109 (2015); doi: 10.1063/1.4917306.

19. M. Turkyilmazoglu, Bödewadt flow and heat transfer over a stretching stationary disk, Int. J. Mech. Sci. 90 (2015) 246-250.

20. M. Mustafa, J. A. Khan, T. Hayat and A. Alsaedi, On Bödewadt flow and heat transfer of nanofluids over a stretching stationary disk, J. Mol. Liq. 211 (2015) 119-125.

21. M. Mustafa, A. Mushtaq, T. Hayat and A. Alsaedi, Rotating flow of magnetite-water nanofluid over a stretching surface inspired by non-linear thermal radiation, PLoS ONE 11 (2016) doi:10.1371/journal.pone.0149304.

22. H. Rosali, A. Ishak, R. Nazar and I. Pop, Rotating flow over an exponentially shrinking sheet with suction, J. Mol. Liq. 211 (2015) 965-969.

23. R. Ahmad and M. Mustafa, Model and comparative study for rotating flow of nanofluids due to convectively heated exponentially stretching sheet, J. Mol. Liq. 220 (2016) 635-641.

24. M. Imtiaz, T. Hayat, A. Alsaedi and B. Ahmad, Convective flow of carbon nanotubes between rotating stretchable disk with thermal radiation effects, Int. J. Heat Mass Transf. 101 (2016) 948-957.

25. I. C. Liu, H. I. Andersson, Heat transfer over a bidirectional stretching sheet with variable thermal conditions, Int. J. Heat Mass Transf. 51 (2008) 4018-4024.

26. M. S. Abel, J. Tawade and M. M. Nandeppanavar, MHD flow and heat transfer for upper-convected Maxwell fluid over a stretching sheet, Meccanica , 47 (2012) 385.

27. M. A. Megahed, Variable fluid properties and variable heat flux effects on the flow and heat transfer in a non-Newtonian Maxwell fluid over an unsteady stretching sheet with slip velocity, Chinese Phys. B 22 (2013) 094701.

28. F. M. Abbasi, M. Mustafa, S. A. Shehzad, M. S. Alhuthali and T. Hayat, Analytical study of Cattaneo-Christov heat flux model for a boundary layer flow of Oldroyd-B fluid. Chinese Phys. B 25 (2016).

29. A. Mushtaq, M. Mustafa, T. Hayat and A. Alsaedi, A numerical study for three-dimensional viscoelastic flow inspired by non-linear radiative heat flux, Int. J. Non-Linear Mech. 79 (2016) 83-87.